Research Article | Vol. 27, No. 20 / 30 September 2019 / Optics Express 27831
Optics EXPRESS

A versatile method for fabricating Pancharatnam-Berry micro-optical elements

JIANGHAO XIONG, TAO ZHAN, AND SHIN-TSON WU*

College of Optics and Photonics, University of Central Florida, Orlando, Florida 32816, USA
swu@creol.ucf.edu

Abstract: We report a simple method for fabricating Pancharatnam-Berry micro-optical elements based on relayed Mach-Zehnder interferometer. Two major advantages are fast processing speed and good quality phase profile. Both active and passive micro-lens arrays are fabricated and their imaging performances characterized. To demonstrate the versatility of the proposed method, we also fabricated asymmetric, axial-symmetric, and concentric types of micro-lens arrays.

© 2019 Optical Society of America under the terms of the OSA Open Access Publishing Agreement

1. Introduction

Optical systems with micro-optics elements have recently found increasing applications in LED light extraction [1,2], lighting [3], imaging [4,5], and light field displays [6–8] due to their unique properties of modulating the light. Among different micro-optical elements, micro-lens array (MLA) receives the greatest attentions due to its excellent imaging abilities. Generally, the fabrication methods of conventional refractive micro-lenses can be categorized into three groups: physical [9–13], chemical [14,15], and direct writing [16,17]. The physical methods have the merits of achieving tunable focal lengths with an applied electric field or mechanical force. Nevertheless, the phase profile of the lens is difficult to control precisely, which in turn causes aberrations and limits the potential uses in high-performance imaging and display systems. Similar problems also exist in chemical methods, combined with limited choices of materials and complex processes. The direct writing method can obtain well-defined phase profile and therefore is attractive for making micro-lenses with excellent optical performance. However, it usually requires point-to-point scanning or shaping so that the overall fabrication time is long and the associated cost is high.

Recently, optical elements based on Pancharatnam-Berry (PB) phase [18,19] have received great interests due to their compact size, polarization selectivity, and high diffraction efficiency [20–23]. The PB phase, also called geometric phase, originates from the difference in the transition process when an incident light evolves from one state to another. The most common PB optical elements are created by patterning the half-wave plate (HWP). If we denote the direction of the optical axis as $\varphi(x,y)$, then the Jones calculus for the incoming circularly polarized light can be expressed as:

$$J_{\pm} = \frac{1}{\sqrt{2}} \begin{bmatrix} \cos 2\varphi & \sin 2\varphi \\ -\sin 2\varphi & \cos 2\varphi \end{bmatrix} \begin{bmatrix} 1 \\ \pm i \end{bmatrix} = e^{\pm i2\varphi} \frac{1}{\sqrt{2}} \begin{bmatrix} 1 \\ \mp i \end{bmatrix}. \quad (1)$$

Besides flipping the handedness of a circularly polarized light, the HWP also adds an extra phase of $2\varphi(x,y)$, which is twice the angle of the optical axis. If we spatially pattern the optical axis of the HWP as Fig. 1(a) depicts, then the overall phase profile (see Fig. 1(b)) would function as a MLA. From Eq. (1), the phase has opposite signs for the left-handed circularly polarized (LCP) light and the right-handed circularly polarized (RCP) light. That means the PB microlens actually has two focal depths corresponding to different polarization states of the input light.

#375139 https://doi.org/10.1364/OE.27.027831
Journal © 2019 Received 12 Aug 2019; revised 8 Sep 2019; accepted 8 Sep 2019; published 18 Sep 2019

Optics EXPRESS

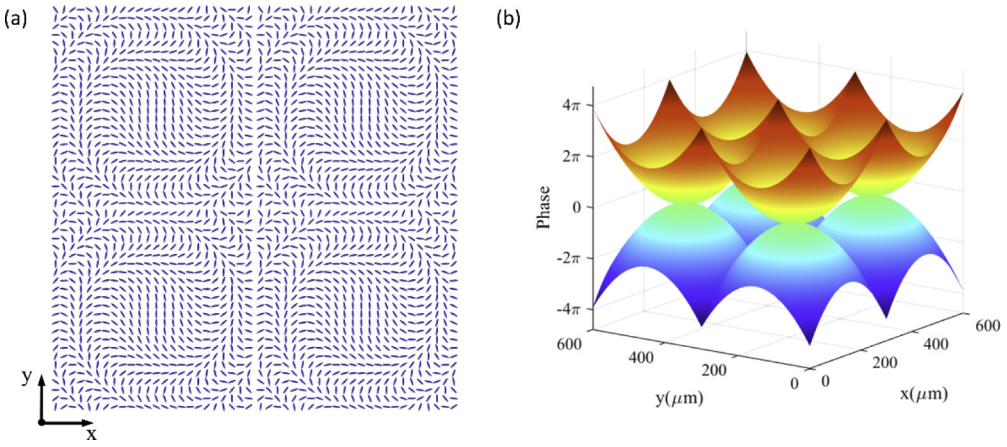

Fig. 1. (a) Pattern of the HWP optical axis in a 2-by-2 PB lens array. (b) Phase profile of the 2-by-2 PB lens array. The upper phase profile (red) corresponds to the LCP light and the bottom (blue) corresponds to the RCP light.

To achieve this type of patterning for the HWP, liquid crystal (LC) combined with photo-alignment technique stands out as a great candidate due to the self-assembly property. The mechanism is based on that when illuminated with a linearly polarized light, the azo-dye molecules tend to reorient perpendicularly to the polarization direction of the light [24,25]. If the linearly polarized light has a certain spatial pattern of polarization direction, then such a pattern will be encrypted into the azo-dye photo-alignment layer. Afterward, a layer of LC (or reactive mesogen) is placed on top of the photo-alignment layer, due to the interaction between the LC molecules and azo-dye molecules, the LC director (the optical axis) will in turn follow the pattern of the photo-alignment layer. If we control the thickness of the LC layer to satisfy the half-wave condition, then the patterned HWP can be fabricated.

A critical issue of fabricating PB optical elements is to create the desired alignment pattern. To do so, several approaches have been reported, including direct writing [26], nanoimprinting [27], projection lithography [28], and interference exposure [20,21,23]. Direct writing method involves spatially moving the focused laser beam and simultaneously changing the polarization direction accordingly to create the arbitrary alignment pattern on the photo-alignment layer. It can produce excellent phase profile but is time-consuming for creating each alignment pattern because of the point-to-point scanning. Nanoimprinting technique adopts a different type of alignment mechanism, which resembles that of the rubbing technique [29,30]. It first uses the laser-writing method to create a master stamp with a groove pattern whose local groove direction is spatially varying. Then it uses the patterned master stamp to transfer the groove pattern to the substrate. The LC on top of the substrate will then also follow the pattern because the grooves give the local LC molecules a preferred orientation, which entails the same operation principle as rubbing technique. This method can have high yield once the imprinting master is created. However, due to the inherent problems of rubbing technique, to get smooth alignment without defects remains a technical challenge. Projection lithography directly projects the linearly polarized pattern formed by a spatial light modulator (SLM) onto a photo-alignment layer. The fabrication process is fast, but the resolution and smoothness of the pattern are limited by the SLM. Interference exposure utilizes the interference of LCP light and RCP light to produce linearly polarized pattern, whose polarization direction is proportional to the phase difference of two optical paths. A commonly used interferometer is Mach-Zehnder (MZ) interferometer due to its convenience to manipulate the phase profile of the light paths. Nevertheless, the focal length of a micro-lens is usually

Optics EXPRESS

quite short, which makes the beam-splitter in MZ interferometer too bulky for fabrication of micro-lens.

In this work, we improve the MZ interferometer with a relay optics to enable the fabrication of PB micro-optics with fast processing speed while keeping a high precision phase profile. To demonstrate feasibility, we fabricated both passive and active MLAs and evaluated their focusing and imaging behaviors. The pitch and focal length of the MLA can also be conveniently adjusted by changing the parameters of the relay optics. To illustrate the versatility of the system further, we also fabricated asymmetric, axial-symmetric, and concentric MLAs, which are difficult to fabricate with conventional methods.

2. Experiment

2.1. Exposure system

Figure 2 depicts the exposure system. The laser used is an OBIS 488-nm LS 60-mW laser from Coherent^{TM} with linear polarization and coherent length of 3 meters. After spatial filtering and expansion, the beam is separated into two arms by the first beam splitter (BS1) to form a MZ interferometer, and the two beams are recombined at BS2. The final beam size on the sample is about 2.5 cm in diameter and the intensity is 1.5 mW/cm^2. The light passing through QWP1 is labelled as path 1 and the other channel as path 2. Path 1 has a relay optics to project the MLA phase profile to the sample position (S) behind BS2. The MLA is refractive type and has plano-convex shape. The lens pitch is $P_0 = 300$ μm and focal length is $F_0 = 18.6$ mm. The relay lenses L1 and L2 are separated by a distance f_1+f_2, where f_1 and f_2 are their corresponding focal lengths. The purpose of such design is to ensure the wavefront of the beam after passing through the relay optics has no curvature. In experiment, we chose the lenses with $f_1 = 15$ cm and $f_2 = 10$ cm. The relayed image of MLA has a magnification ratio of $M = f_2/f_1$, and the image distance d_2 satisfies the following relation:

$$f_1\frac{d_2}{f_2} + f_2\frac{d_1}{f_1} = f_1 + f_2. \tag{2}$$

In experiment, we set $d_1 = f_1 = 15$ cm, so from Eq. (1) we find $d_2 = f_2 = 10$ cm. This means the distance between the second lens and the final image is sufficiently large for placing a beam splitter in between. After the relay optics, the beam size also changes according to the magnification ratio, which means the light intensity also changes. Therefore, we inserted a linear polarizer in path 1 to equalize the output light intensities from two arms. The reason we put the linear polarizer in path 1 is that in our case the light intensity after the relay optics increases. If the relay optics decreases the light intensity, then the linear polarizer should be placed in path 2 instead.

The light in path 2 acts as the reference beam for forming interference. Generally, there is no additional optical component placed in path 2 (box A in Fig. 2) in order to get a normal MLA phase profile. However, a proper modification can be made to achieve unconventional MLA phase profiles. For example, if a wedge is added, or alternatively the mirror M2 is rotated, then the MLA phase profile would have an additional linear phase profile, making the fabricated PB MLA asymmetric. If a lens or a cylindrical lens is added, then the final PB MLA would have an additional parabolic phase profile in two or one dimension, which makes it concentric or axial-symmetric. Some examples will be illustrated later.

2.2. Fabrication process

In experiment, we fabricated two types of PB MLAs: passive and active. The passive type adopts reactive mesogen, which has similar properties to LCs and can be polymerized with UV light. The active type uses a nematic LC whose orientation can be tuned by an electric field. Figure 3 depicts the detailed fabrication procedures. It should be clarified that for the passive type we used normal glass substrates, while for the active type we used ITO-coated glass substrates. In both

Optics EXPRESS

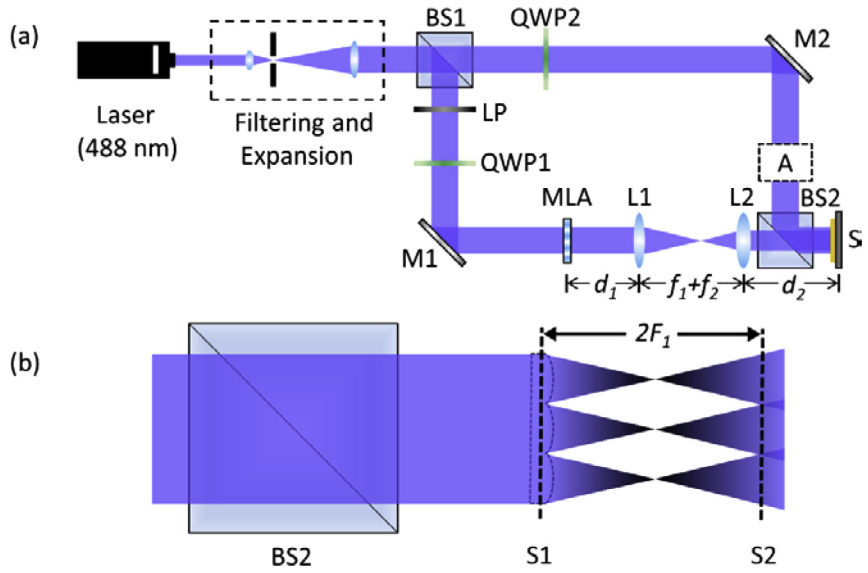

Fig. 2. (a) Schematic plot of the exposure system. BS1 and BS2: non-polarizing beam splitters; QWP1 and QWP2: quarter-wave plates; M1 and M2: dielectric mirrors; LP: linear polarizer; MLA: micro-lens array: L1 and L2: relay lenses; S: sample coated with a thin photo-alignment material (brilliant yellow). The box A indicates the potential change in the reference beam, which could be a wedge, a cylindrical lens, a lens or nothing. (b) Detailed plot of the possible positions (S1 and S2) behind BS2 to place the sample S. The dashed profile stands for the relayed image of the MLA. F_1 is the focal length of the relayed MLA profile. For clearance, the reference beam is not plotted.

cases, the first step was to clean the glass substrate with ethanol, acetone, and isopropyl-alcohol. Next, we spin-coated a thin layer of photo-alignment material brilliant yellow (from Tokyo Chemical Industry, 0.2 wt.% in dimethyl-formamide) onto the substrate at 500 rpm ramp for 5s followed by 3000 rpm for 30s. After that, we placed the sample in the exposure system for 5 min, so the total dosage was about ~ 0.5 J/cm^2 with the measured light intensity at 1.5 mW/cm^2.

To make a passive MLA, we spin-coated a layer of reactive mesogen mixture (RMM) onto the substrate. The RMM consisted of 3 wt.% photo-initiator Irgacure 651 (from BASF), 1% surfactant Zonyl 8857A (from DuPont), and 96% RM257 (from LC Matter). The employed surfactant was to improve the surface quality of the MLA. The RMM was diluted in toluene with 1:4.3 weight ratio to form the RMM solution. The spin-coating condition was also 500-rpm ramp for 5s and 3000-rpm for 30s in order to control the LC monomer thickness to satisfy the half-wave condition. Finally, we cured the sample under UV light (356 nm) with a dosage of ~3J/cm^2 (5 min with ~10 mW/cm^2 power density) in nitrogen-rich environment, forming the cross-linked polymer network. Detailed fabrication procedures can be found in [31].

For the active MLA, we used another clean glass substrate and assembled a LC cell using the substrate with patterned BY layer. The cell gap was controlled to be 2 μm to satisfy the half-wave condition of our LC material. The LC material (DIC-LC2) was then infiltrated into the cell. The reason for using DIC-LC2 is due to its ultra-low viscosity for achieving fast response time [32]. After the infiltration, we heated the sample to an isotropic phase (100°C) and gradually cooled it down to the room temperature (~22°C). The data of both the passive and active MLAs are listed in Table 1.

Optics EXPRESS

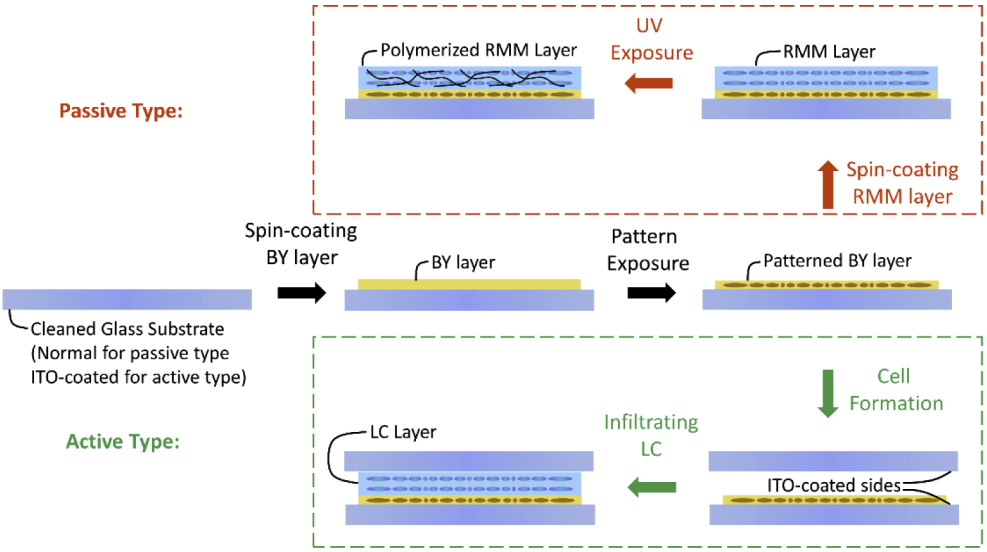

Fig. 3. Fabrication flowchart of passive (red arrows and box) and active (green arrows and box) PB MLAs. BY: brilliant yellow; RMM: reactive mesogen mixture.

Table 1. Properties of the materials for the passive and active PB MLAs.

Cell Type	Material	Δn	Thickness	γ_1/K_{11}	Δε
Passive	RM257	0.18	1.4 μm	-	-
Active	DIC-LC2	0.12	2.1 μm	2.6 ms/μm^2	2.0

3. Results and discussion

3.1. Passive PB MLA

For the exposure part, there actually exists two possible planes for putting the photo-alignment layer. The first plane, plane 1 (S1 in Fig. 1(b)), is at the exact relayed image of the MLA. The second plane, plane 2 (S2 in Fig. 1(b)), is at the plane with a shift of $2F_i$ with respect to the first plane, where F_i is the focal length of the relayed image of the MLA and can be calculated as $F_i = F_0 f_2/f_1 = 12.4$ mm. Both schemes are carried out in the experiment and the passive PB MLAs are fabricated accordingly. The phase profiles of the fabricated passive MLAs under polarization optical microscope with crossed linear polarizers are shown in Figs. 4(a)–4(d). The adjacent dark fringes correspond to a phase change of π [31].

For the fabrication of a normal PB lens, the phase profiles at planes 1 and 2 are identical. Thus, placing the sample at $2F$ distance (S2 in Fig. 1(b)) generates good results [20]. However, it is obvious that the MLA sample placed at plane 1 (Figs. 4(a) and 4(b)) has a much better phase profile than the sample at plane 2 (Figs. 4(c) and 4(d)). For detailed analysis, in Fig. 4(e) we also plotted the extracted phase profile along the blue dashed line in Fig. 4(b). The theoretical phase is calculated using following formula:

$$\phi_t = \frac{2\pi}{\lambda}\left(\sqrt{x^2 + {F_i}^2} - F_i\right), \tag{3}$$

where λ is the wavelength. In this calculation, we use λ=532 nm. Good agreement between experiment and theory is observed, as Fig. 4(e) shows. The difference between the phase quality of samples placed at plane 1 and plane 2 results from the diffraction effect of the lens array from the 2D periodic pattern. For a simple estimation, we use the far-field diffraction formula and

Optics EXPRESS

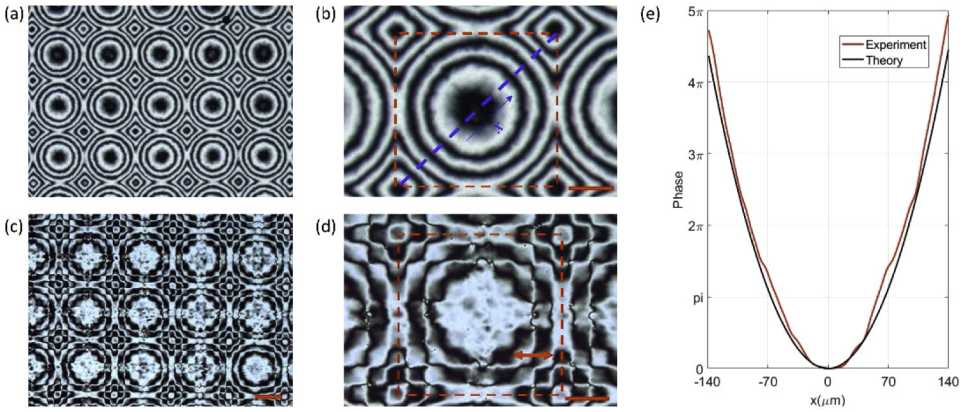

Fig. 4. Phase profiles of the passive MLAs under a polarizing optical microscope under crossed linear polarizers. (a), (b) Phase profiles with sample at plane 1. (c), (d) Phase profiles with sample at plane 2. The scale bar in (a) and (c) is 100 μm, and in (b) and (d) is 50 μm. (e) Comparison of the experimental phase profile extracted from the data along the blue dashed line in (b) and theoretical phase profile.

calculate the fringe period as $P_f = 2F_i\lambda/P = 64\ \mu m$ for λ=532 nm. The period corresponds to the length of the red arrow shown in Fig. 4(d) because the period of PB optical elements is half as the period of the interference pattern. The calculation agrees with experiment very well.

This difference also suggests if we want to fabricate a PB MLA with a good phase profile, the relay of the original phase is quite necessary because the phase profile at $2F_i$ plane can be corrupted due to the diffraction effect of the array. From here on, all our fabricated samples are placed at plane 1.

3.2. *Focusing, imaging, and switching ability*

To examine the focusing behavior, we place the sample under microscope with collimated light from a halogen lamp. Filters with bandwidth of about 5 nm are applied for producing red, green and blue lights. Results are shown in Figs. 5(a)–5(d). To further understand the spectral performance, we also measured the transmission spectrum (zero-order leakage) with the MLA sandwiched between RCP and LCP polarizers. The spectrometer is Ocean Optics model HR4000CG-UV-NIR. The first-order diffraction efficiency, defined as one minus the zero-order leakage [33], is plotted in Fig. 5(e). The thickness of the MLA is controlled so that it has the highest efficiency at green light, which corresponds to the highest efficiency at around 515 nm in Fig. 5(e). It should be noted that due to the different bandwidths of the filters and spectrum of the halogen lamp, the red light (633 nm) has the highest light intensity, then the blue (450 nm) and green (546 nm) lights. Therefore, Fig. 5(a) appears to have the brightest focus point while Fig. 5(b) is the darkest. This comes from the light source and is not an indicator of the efficiency of the MLA. The efficiency should be determined by the contrast of the focusing point to the background. From Figs. 5(a)–5(d), the green light has the highest contrast, while the red and blue light has some light leakage in the background due to the decreased efficiency. However, this behavior comes from the fact that the PB MLA consists of only one layer and therefore the wave-plate efficiency is dependent on the wavelength. Achromatic focusing efficiency can be achieved by introducing a dual-twist structure [23].

The active PB MLA basically has the same configuration as the passive one, except for replacing the LC polymer (RM257) with a LC mixture (DIC-LC2). Therefore, the active PB MLA has the same optical performance as the passive one, except for the dynamic switching

Optics EXPRESS

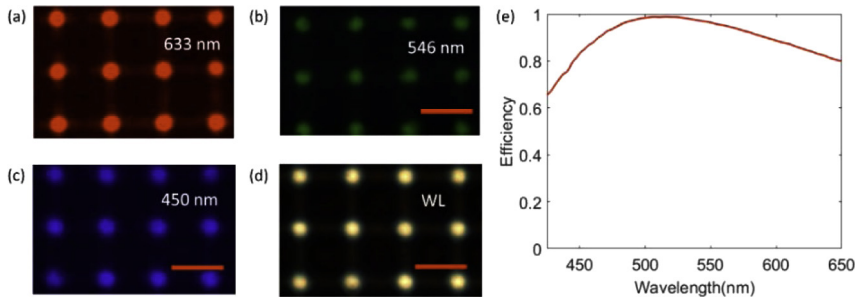

Fig. 5. Focusing performance of the passive PB MLA at (a) 633 nm, (b) 546 nm, (c) 450 nm and (d) white light with no filter. Scale bars: 200 μm. (e) Efficiency spectrum from the measured transmittance of the MLA sandwiched between RCP and CLP polarizers.

property. The threshold voltage of our fabricated cell is $6V_{rms}$. Figure 6(a) depicts the measured response time: rise time ≈ 1.05 ms and fall time ≈ 1.57 ms. We also demonstrated the switching behavior with an object shown in Fig. 6(b). The MLA is placed at ~1-cm away from the object. To enhance the image contrast, we added a circular polarizer on top of the MLA. The image is shown in Fig. 6(c), with each image of the object corresponding to a single lenslet in the MLA. When we applied $7V_{rms}$ to the cell, the vertical electric field exerts a torque to reorient the LC directors perpendicular to the substrates. Therefore, the original MLA pattern is erased and the lensing effect disappears, making the image completely out of the focus, as Fig. 6(d) shows.

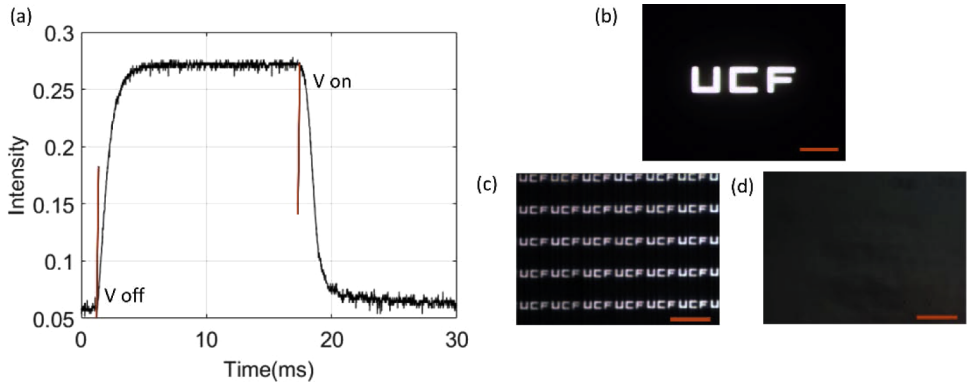

Fig. 6. Switching behavior of the active PB MLA. (a) Response time curve with an applied voltage of $7V_{rms}$. (b) Imaging object. (c) The image with MLA placed at 1-cm distance from the object, with no applied voltage. (d) Image with applied voltage ($7\ V_{rms}$). Scale bars: 200 μm.

3.3. *Asymmetric, axial-symmetric, and concentric MLA*

Aside from normal MLA, other MLA derivatives can be fabricated by modifying the wavefront of the reference beam. When we adjust the mirror in the reference beam path (M2 in Fig. 2), the MLA phase profile will be superimposed with a linear phase, which makes the MLA asymmetric, as shown in Figs. 7(a) and 7(b). The rotation angle of the mirror determines the degree of asymmetry.

When a cylindrical lens ($F_c = 10$ cm) is placed in the reference beam, the reference beam on the sample will have a wavefront curvature in one dimension. In experiment, the cylindrical lens was placed such that the distance from the sample to the beam splitter (BS2 in Fig. 2) combined

Optics EXPRESS

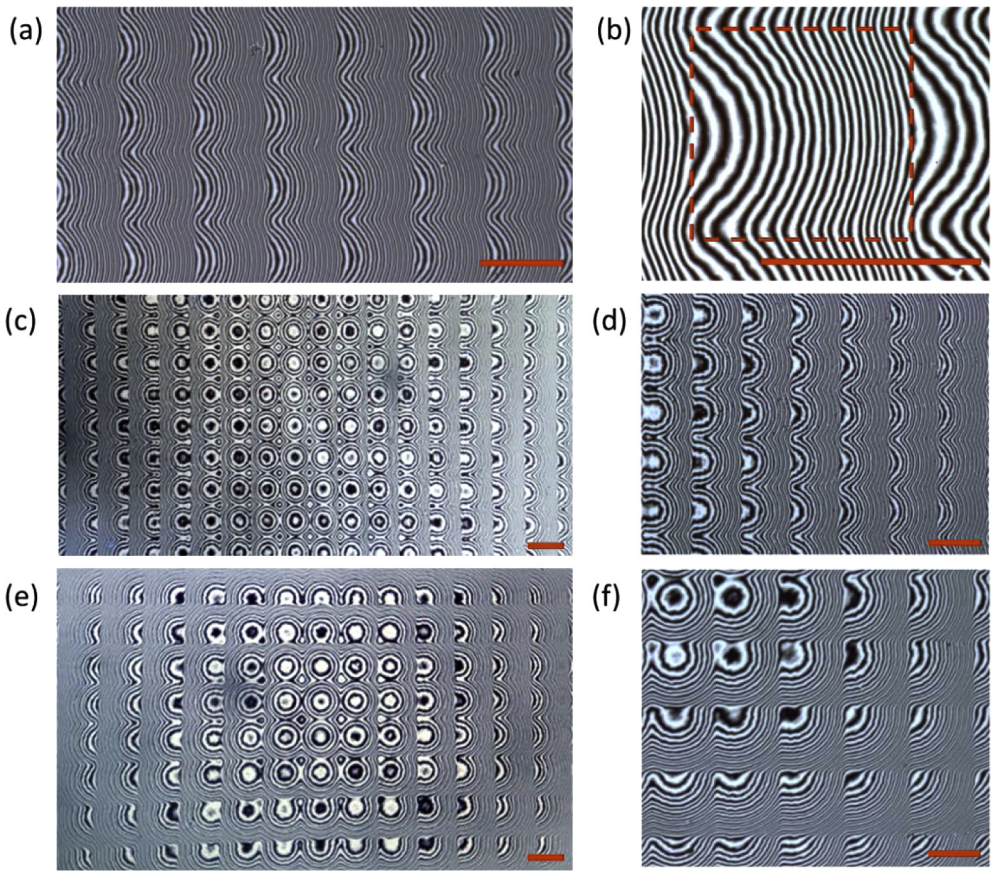

Fig. 7. Phase profile of derivative MLAs under polarizing microscope with crossed linear polarizers. (a) and (b): Asymmetric MLA by adjusting the incident angle of reference beam. (c) and (d): Axial-symmetric MLA by placing a cylindrical lens in the reference beam path. (e) and (f): Concentric MLA by placing a lens in the reference beam path. Scale bars: 200 μm.

with the distance from the cylindrical lens (box A in Fig. 2) to the beam splitter (BS2 in Fig. 2) equals to $2F_c$. In this way, the light intensity of the reference beam is unchanged compared to the setup without the lens. The curvature of the wavefront on the sample is identical to the one induced by the cylindrical lens itself. However, this placement at $2F_c$ is not absolutely necessary because a linear polarizer can be added in the reference beam to adjust the light intensity as well. That is, if we place the cylindrical lens at a place closer to the beam splitter (BS2 in Fig. 2), both wavefront curvature and light intensity of the reference beam increase. Then we can adjust the linear polarizer in the reference beam to make the light intensity in both paths equal again. This way we can arbitrarily change the wavefront curvature of the reference beam while maintaining the same intensity for both beams. The MLA phase profile combined with the one-dimensional parabolic phase profile produces the axial-symmetric MLA shown in Figs. 7(c) and 7(d). The asymmetry of the micro-lens profile increases when it is further away from the central line. This means that the lenses not only focus the light, but also guide the focused beam toward the central line. Therefore, the axial-symmetric MLA manifests two focal lengths. The first focal length F_1 is the one of the lenslets, which is the same as F_i, while the second focal length F_2 depicts the convergence of the light bundles passing through the lenslets. In our experiment, F_2 is equal to

Optics EXPRESS

the focal length of the cylindrical lens F_c, but it can be adjusted using the method described above. In Fig. 7(c), some nonuniformity is observed in the lens patterns, which originates from the misalignment between the reference beam direction and relay beam direction after introducing the lens. In other words, a small error linear profile is added into the pattern. However, the general effect of the error linear profile should be negligible.

When a lens ($F_l = 10$ cm) is placed in the reference beam path instead, the parabolic phase profile becomes two-dimensional. The overall MLA phase profile becomes concentric, as shown in Figs. 7(e) and 7(d). In experiment, we also placed the lens at $2F_l$ distance from the sample. The above discussion with the cylindrical lens works the same here. Due to the ability to converge the imaging rays, the axial-symmetric and concentric MLAs can be used in, for example, integral imaging display systems to replace the curved MLA and display screen for widening the viewing angle [7,8]. The compact form factor of our MLA is also highly desirable for practical applications in the near-eye displays in comparison with the curved ones.

These unconventional MLAs are typically difficult to fabricate using chemical or physical method. Even for the projection lithography and nano-imprinting technique for fabricating arbitrary PB optical elements, the fabrication is also difficult because the periodicity of fringes in those patterns can be very small (Fig. 7), which poses challenges for the resolution of writing machine and spatial light modulator. To the best of our knowledge, this is the first demonstration for fabricating these types of MLAs.

4. Conclusion

A simple method to fabricate PB MLA using MZ interferometer with relay optics is proposed. The method has fast processing speed, high quality of the phase profile, and good versatility. Both passive and active MLAs are fabricated and evaluated in terms of imaging, focusing, and switching ability. Derivative MLAs are also fabricated by adjusting the reference beam wavefront.

Funding

Intel Corporation.

References

1. S. Möller and S. R. Forrest, "Improved light out-coupling in organic light emitting diodes employing ordered microlens arrays," J. Appl. Phys. **91**(5), 3324–3327 (2002).
2. J. H. Lee, Y. H. Ho, K. Y. Chen, H. Y. Lin, J. H. Fang, S. C. Hsu, J. R. Lin, and M. K. Wei, "Efficiency improvement and image quality of organic light-emitting display by attaching cylindrical microlens arrays," Opt. Express **16**(26), 21184–21190 (2008).
3. X. H. Lee, I. Moreno, and C. C. Sun, "High-performance LED street lighting using microlens arrays," Opt. Express **21**(9), 10612–10621 (2013).
4. A. Orth and K. Crozier, "Microscopy with microlens arrays: high throughput, high resolution and light-field imaging," Opt. Express **20**(12), 13522–13531 (2012).
5. K. C. Kwon, M. U. Erdenebat, Y. T. Lim, K. I. Joo, M. K. Park, H. Park, J. R. Jeong, H. R. Kim, and N. Kim, "Enhancement of the depth-of-field of integral imaging microscope by using switchable bifocal liquid-crystalline polymer micro lens array," Opt. Express **25**(24), 30503–30512 (2017).
6. H. Huang and H. Hua, "High-performance integral-imaging-based light field augmented reality display using freeform optics," Opt. Express **26**(13), 17578–17590 (2018).
7. Y. Kim, J. H. Park, H. Choi, S. Jung, S. W. Min, and B. Lee, "Viewing-angle-enhanced integral imaging system using a curved lens array," Opt. Express **12**(3), 421–429 (2004).
8. J. S. Jang and B. Javidi, "Depth and lateral size control of three-dimensional images in projection integral imaging," Opt. Express **12**(16), 3778–3790 (2004).
9. J. T. Wu, W. Y. Chang, and S. Y. Yang, "Fabrication of a nano/micro hybrid lens using gas-assisted hot embossing with an anodic aluminum oxide (AAO) template," J. Micromech. Microeng. **20**(7), 075023 (2010).
10. M. He, X. Yuan, J. Bu, and W. C. Cheong, "Fabrication of concave refractive microlens arrays in solgel glass by a simple proximity-effect-assisted reflow technique," Opt. Lett. **29**(9), 1007–1009 (2004).
11. A. Werber and H. Zappe, "Tunable microfluidic microlenses," Appl. Opt. **44**(16), 3238–3245 (2005).
12. H. Ren, Y. H. Fan, and S. T. Wu, "Liquid-crystal microlens arrays using patterned polymer networks," Opt. Lett. **29**(14), 1608–1610 (2004).

Optics EXPRESS

13. N. R. Smith, L. Hou, J. Zhang, and J. Heikenfeld, "Fabrication and demonstration of electrowetting liquid lens arrays," J. Disp. Technol. **5**(11), 411–413 (2009).
14. K. Lee, W. Wagermaier, A. Masic, K. P. Kommareddy, M. Bennet, I. Manjubala, S.-W. Lee, S. B. Park, H. Cölfen, and P. Fratzl, "Self-assembly of amorphous calcium carbonate microlens arrays," Nat. Commun. **3**, 725 (2012)..
15. B. Hao, H. Liu, F. Chen, Q. Yang, P. Qu, G. Du, J. Si, X. Wang, and X. Hou, "Versatile route to gapless microlens arrays using laser-tunable wet-etched curved surfaces," Opt. Express **20**(12), 12939–12948 (2012).
16. Z. Zhu, S. To, and S. Zhang, "Large-scale fabrication of micro-lens array by novel end-fly-cutting-servo diamond machining," Opt. Express **23**(16), 20593–20604 (2015).
17. R. Guo, S. Xiao, X. Zhai, J. Li, A. Xia, and W. Huang, "Micro lens fabrication by means of femtosecond two photon photopolymerization," Opt. Express **14**(2), 810–816 (2006).
18. S. Pancharatnam, "Generalized theory of interference and its applications," Proc. - Indian Acad. Sci., Sect. A **44**(6), 398–417 (1956).
19. M. V. Berry, "Quantal phase factors accompanying adiabatic changes," Proc. R. Soc. London, Ser. A **392**(1802), 45–57 (1984)..
20. Y. H. Lee, G. Tan, T. Zhan, Y. Weng, G. Liu, F. Gou, F. Peng, N. V. Tabiryan, S. Gauza, and S. T. Wu, "Recent progress in Pancharatnam–Berry phase optical elements and the applications for virtual/augmented realities," Opt. Data Process. Storage **3**(1), 79–88 (2017)..
21. T. Zhan, J. Xiong, G. Tan, Y. H. Lee, J. Yang, S. Liu, and S. T. Wu, "Improving near-eye display resolution by polarization multiplexing," Opt. Express **27**(11), 15327–15334 (2019).
22. G. Tan, T. Zhan, Y. H. Lee, J. Xiong, and S. T. Wu, "Polarization-multiplexed multiplane display," Opt. Lett. **43**(22), 5651–5654 (2018).
23. C. Oh and M. J. Escuti, "Achromatic diffraction from polarization gratings with high efficiency," Opt. Lett. **33**(20), 2287–2289 (2008).
24. M. Schadt, K. Schmitt, V. Kozinkov, and V. Chigrinov, "Surface-induced parallel alignment of liquid crystals by linearly polymerized photopolymers," Jpn. J. Appl. Phys. **31**(Part 1), 2155–2164 (1992).
25. V. G. Chigrinov, V. M. Kozenkov, and H. S. Kwok, *Photoalignment of Liquid Crystalline Materials: Physics and Applications* (Wiley, 2008).
26. J. Kim, Y. Li, M. N. Miskiewicz, C. Oh, M. W. Kudenov, and M. J. Escuti, "Fabrication of ideal geometric-phase holograms with arbitrary wavefronts," Optica **2**(11), 958–964 (2015).
27. Z. He, Y. H. Lee, R. Chen, D. Chanda, and S. T. Wu, "Switchable Pancharatnam-Berry microlens array with nano-imprinted liquid crystal alignment," Opt. Lett. **43**(20), 5062–5065 (2018).
28. L. De Sio, D. E. Roberts, Z. Liao, S. Nersisyan, O. Uskova, L. Wickboldt, N. Tabiryan, D. M. Steeves, and B. R. Kimball, "Digital polarization holography advancing geometrical phase optics," Opt. Express **24**(16), 18297–18306 (2016).
29. N. A. J. M. van Aerle, M. Barmentlo, and R. W. J. Hollering, "Effect of rubbing on the molecular orientation within polyimide orienting layers of liquid crystal displays," J. Appl. Phys. **74**(5), 3111–3120 (1993).
30. J. H. Kim, M. Yoneya, and H. Yokoyama, "Tristable nematic liquid-crystal device using micropatterned surface alignment," Nature **420**(6912), 159–162 (2002).
31. T. Zhan, J. Xiong, Y. H. Lee, R. Chen, and S. T. Wu, "Fabrication of Pancharatnam-Berry phase optical elements with highly stable polarization holography," Opt. Express **27**(3), 2632–2642 (2019).
32. Z. Luo, F. Peng, H. Chen, M. Hu, J. Li, Z. An, and S. T. Wu, "Fast-response liquid crystals for high image quality wearable displays," Opt. Mater. Express **5**(3), 603–610 (2015).
33. N. V. Tabiryan, S. V. Serak, S. R. Nersisyan, D. E. Roberts, B. Y. Zeldovich, D. M. Steeves, and B. R. Kimball, "Broadband waveplate lenses," Opt. Express **24**(7), 7091–7102 (2016).

63.235.172.153 {ts '2019-09-18 20:34:49'}